Different styles of continental delamination: the influence of the viscosity structure and radiogenic heat production

J. L. VALERA[1] & A.M. NEGREDO[1,2]

[1] Departamento de Física de la Tierra, Astronomía y Astrofísica-I, Facultad de CC. Físicas, Plaza de Ciencias 1. 28040-Madrid, Spain. (jlvalera@fis.ucm.es) (anegredo@fis.ucm.es).
[2] Instituto de Geociencias (CSIC-UCM), Facultad de CC. Físicas, Plaza de Ciencias 1. 28040-Madrid, Spain.

Recibido: 28/07/2011
Aceptado: 4/10/2011

Resumen
En este estudio se aplican algoritmos termomecánicos para modelizar la evolución asimétrica de una litosfera orogénica engrosada, con un conducto adyacente de baja viscosidad, que atraviesa la litosfera. Analizamos la influencia en la evolución de la delaminación de la estratificación de viscosidad, de la producción radiogénica de calor y de la naturaleza del material presente en el conducto de baja viscosidad. Esta evolución es muy sensible a la viscosidad del manto litosférico y, en menor grado, a la viscosidad de la astenosfera y de la corteza inferior. Un aumento de tan sólo un orden de magnitud de la viscosidad máxima permitida para la litosfera (de 10^{22} a 10^{23} Pa s) produce un cambio de una delaminación bien desarrollada, con una fuerte migración del punto de delaminación, a una completa inhibición del proceso.
Los resultados muestran que la producción radiogénica de calor tiene una fuerte influencia en la geometría del manto litosférico en hundimiento. Los modelos con una elevada producción de calor en la corteza inferior predicen el ascenso astenosférico, sin que se forme una estructura de tipo *slab* en el manto superior.
Obtenemos que la naturaleza del material que constituye el conducto de baja viscosidad, bien sea material astenosférico o bien manto litosférico de baja viscosidad, no afecta significativamente al proceso de delaminación. Sugerimos que tanto el debilitamiento litosférico por procesos de deshidratación como el adelgazamiento térmico son mecanismos plausibles para la formación de conductos de baja viscosidad capaces de desencadenar la delaminación.

Palabras clave: Delaminación, estratificación de viscosidad, producción radiogénica de calor, modelización termomecánica.

Diferentes estilos de delaminación continental: influencia de la estructura de viscosidad y de la producción radiogénica de calor.

Abstract
Thermo-mechanical algorithms are applied in this study to model the asymmetric evolution of a thickened orogenic lithosphere with an adjacent 'low viscosity conduit' across the lithosphere. We investigate the influence of viscosity stratification, crustal radiogenic heat production, and nature of the material filling the 'low viscosity conduit' on the evolution of delamination. This evolution is shown here to be very sensitive to the lithospheric mantle viscosity and, to a lesser degree, to asthenosphere and lower crust viscosities. An increase of only one order of magnitude in the maximum

viscosity of the lithospheric mantle (from 10^{22} to 10^{23} Pa s) causes a change from a well-developed delamination with large displacement of delamination point to a complete inhibition of this process.
Radiogenic heat production is shown to have a strong influence on the resulting geometry of the sinking lithospheric mantle. Models with high radiogenic heat production in lower crust reproduce asthenospheric upwelling but without creating a slab-like structure in the upper mantle.
We obtain that the nature of the material filling the low viscosity conduit, either asthenospheric material or low viscosity lithospheric mantle, does not significantly affect the development of delamination. We suggest that both lithospheric weakening by dehydration processes and thermal thinning processes are plausible mechanisms for the formation of 'low viscosity conduits' able to sustain delamination.

Keywords: Delamination, viscosity stratification, radiogenic heat production, thermo-mechanical modeling.

Referencia normalizada
Valera, J. L. Negredo, A. M., (2011). Different styles of continental delamination: the influence of the viscosity structure and radiogenic heat production. *Física de la Tierra* Vol. 23 Núm. 1 (2011): 113-130

Introduction

Continental delamination and convective removal are geodynamic mechanisms commonly proposed to explain observations likely related to the rapid thinning of continental lithospheric mantle. Significant observations are anomalously high heat flow, regional uplift, change of stress field toward extension, and the presence of cold slabs in the upper mantle and igneous activity in continental areas far from present subduction zones.

The convective removal mechanism is based on the development of gravitational instabilities at the base of the lithospheric mantle (e.g. Houseman et al., 1981; England and Houseman, 1989). The concept of continental delamination was introduced by Bird (1978, 1979), who proposed that the dense lithospheric mantle might peel off the crust and sink into the underlying asthenosphere, as soon as any process provided an elongated 'asthenospheric conduit' connecting the asthenosphere with the base of the continental crust. Differently from convective removal, which is accommodated by viscous dripping, the delaminated mantle part of the lithosphere peels away as a coherent slice, without necessarily undergoing major internal deformation, and is replaced by buoyant asthenosphere. Another significant difference between delamination (as originally proposed by Bird) and convective removal is that the former implies a lateral migration of the point of delamination, where the lithospheric mantle peels off the overlying crust.

Morency and Doin (2004) presented a thorough study where they investigated by means of thermo-mechanical numerical simulations the conditions for the initiation and propagation of continental delamination. In the modeling by Morency and Doin (2004), delamination begins with the spontaneous development of strong lithospheric mantle thinning in a narrow area (about 100 km wide); then the hori-

leads to mantle lithosphere sinking into the convective mantle. Although Morency and Doin (2004) discussed the effect of the Moho temperature on the development of delamination, they did not analyze the crustal deformation resulting from this process nor investigated causes for the increased Moho temperature other than crust thickness. On the other hand, some studies (Schott and Schmelling 1998; Göğüş and Pysklywec, 2008; and Valera et al. ,2008; 2011) introduced an initial setup 'ad hoc' to develop delamination by including a weak area playing the role of 'asthenospheric conduit' and an area of negatively buoyant lithospheric mantle. These studies highlighted the important implications of the lateral propagation of delamination on resulting lithospheric structure, paying special attention to the crustal structure and near surface observables as surface heat flow and topography.

We focus here on the analysis of the physical conditions that enable this lateral propagation to occur. In particular we aim to study the influence of viscosity stratification, as well as the influence of the initial thermal regime, as controlled by crustal radiogenic heat production, on the resulting upper mantle structure. In this sense, this study is complementary to the studies by Valera et al. (2008; 2011) and Göğüş and Pysklywec (2008), but rather than focusing on near surface and crustal-scale consequences, we will discus the effects of rheologic stratification and initial geotherm on upper mantle structure.

1. Methodology

1.1 Modeling description

We have followed the methodology presented by Valera et al. (2008, 2011) which has been shown to be useful to model viscous processes as the continental delamination. This methodology simplifies the coupled equations of mass, momentum and energy by assuming two-dimensional flow, neglecting inertial forces and shear heating, and considering the Boussinesq approximation but including the thermal effects of compression. These assumptions lead to the final equations:

$$\frac{\partial}{\partial x}\left(\rho g\right) = 4\frac{\partial^2}{\partial x \partial z}\left[\mu\frac{\partial^2}{\partial x \partial z}\Psi\right] + \left(\frac{\partial^2}{\partial z^2} - \frac{\partial^2}{\partial x^2}\right)\left[\mu\left(\frac{\partial^2}{\partial z^2} - \frac{\partial^2}{\partial x^2}\right)\Psi\right] \tag{1}$$

$$\frac{\partial T}{\partial t} + u_x\frac{\partial T}{\partial x} + u_z\frac{\partial T}{\partial z} = \frac{H}{C_P} + \frac{k}{\rho C_P}\left(\frac{\partial^2 T}{\partial x^2} + \frac{\partial^2 T}{\partial z^2}\right) + u_z\frac{\alpha g}{C_P}T \tag{2}$$

where u_k is the k-component of the velocity vector; x is the horizontal coordinate; z is the vertical coordinate, pointing downward; μ is the viscosity; ρ is the density; g is the acceleration of gravity; C_p, the specific heat; T, the temperature; t is the time; H, the radiogenic heat production; k, the thermal conductivity; α, the thermal expansion coefficient. The velocity is related to the stream function Ψ as:

$$u_x = \frac{\partial\Psi}{\partial z}; \quad u_z = -\frac{\partial\Psi}{\partial x} \tag{3}$$

The heat equation (2) includes the following heat sources: the radiogenic heat production, the heat conduction and the adiabatic heating. The values of the parameters used are listed in Table 1. See Valera et al. (2008) for further details on the mathematical developments.

To numerically solve the governing equations, we have used the MATLAB finite difference code developed by Valera et al. (2008; 2009), The surface temperature is fixed at 0ºC, a constant heat-flow computed from the initial geotherm is forced at the bottom, and zero horizontal heat flow at the side boundaries (figure 1a). A free slip condition is applied at all boundaries.

We have used two different grids: an Eulerian grid with fixed nodes and a Lagrangian grid with moving markers carrying the material properties. The Eulerian grid is a Cartesian box with an aspect ratio of about 2 (1376×680 km), and a resolution of 173×86 nodes in the x- and z directions). The Lagrangian grid has three times more markers than nodes in each direction. The convergence of the results has been checked varying the spatial and time resolution and controlling the Courant criterion (e.g. Anderson, 1995).

Table 1: Fixed parameters used in all calculations

Symbol	Meaning	Value
g	Acceleration of gravity	9.8 m s^{-2}
Q_b	Basal heat flow	0.014 W m^{-2}
b	b-parameter of viscosity Law	15
H_p	Crustal radiogenic heat production	variable
L	Lithospheric thickness	116 km
	Lower bound for the viscosity	10^{17} Pa s
$h_{\_LC}$	Lower Crust thickness	24 km
	Maximum depth of the Lithospheric Mantle perturbation	244 km
	Maximum depth of the Lower Crust perturbation	68 km
	Maximum depth of the Upper Crust perturbation	28 km
μ_{max}	Maximum for the mantle viscosity	$2.5x10^{22}$ Pa s
ρ_{LC}	Orogenic Lower Crust density	3050 kg m^{-3}
x_{pert}	Position of the perturbation	688 km
c_p	Specific heat	1.3×10^{3} J K^{-1} kg^{-1}
T_0	Temperature at the base of the lithosphere	1350 ºC
k	Thermal conductivity	3.2 W m^{-1} K^{-1}
α	Thermal expansion coefficient	3.7×10^{-5} K^{-1}

	Time step	0.25 Ma
$h_{\_UC}$	Upper Crust thickness	12 km
ρ_{UC}	Upper Crust density	2800 kg m^{-3}
μ_{UC}	Upper Crust viscosity	10^{23} Pa s
ρ_{LM}	Lithospheric Mantle density	$3400[1-\alpha(T-T_0)]$ kg m^{-3}
ρ_{AS}	Asthenospheric density	$3400[1-\alpha(T-T_0)]$ kg m^{-3}
ρ_{npLC}	Lower Crust density (non perturbed zone)	2900 kg m^{-3}
μ_{npLC}	Lower Crust viscosity (non perturbed zone)	10^{20} Pa s

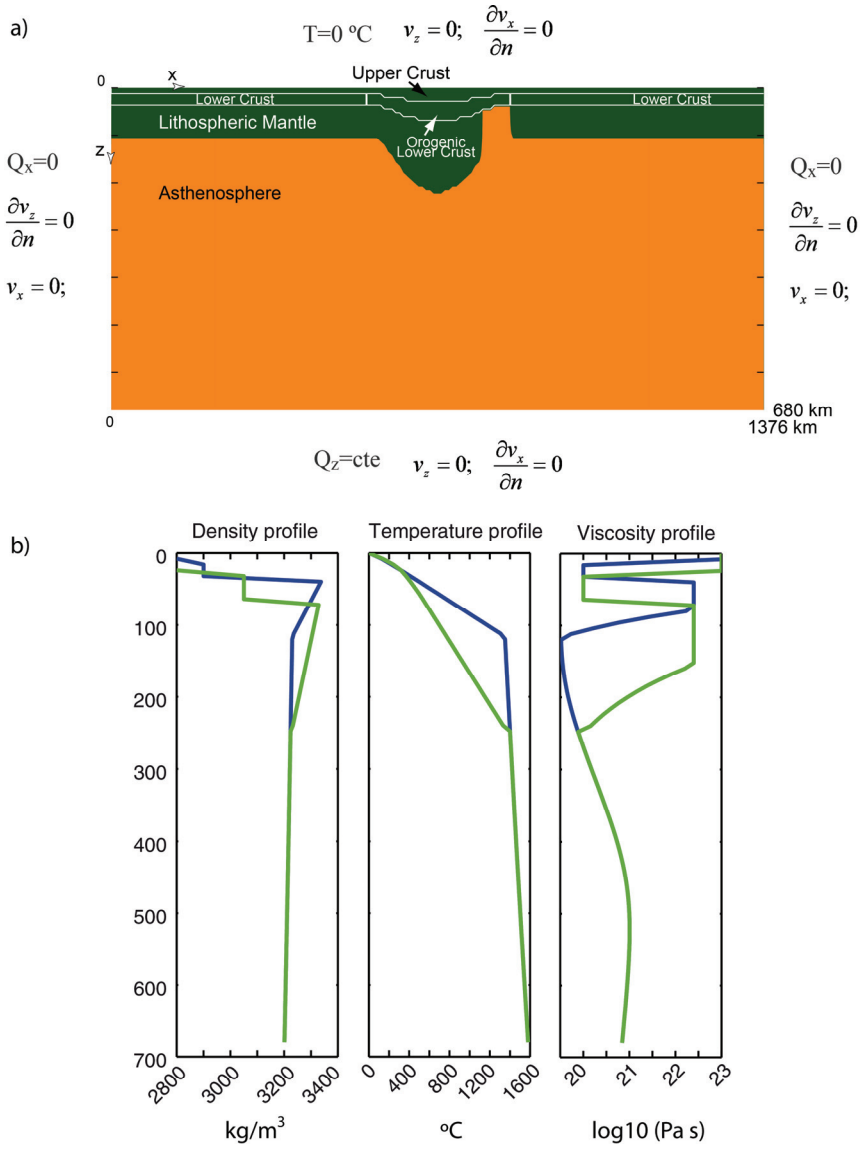

Figure 1: a) Model domain illustrating the initial geometry and boundary conditions. b) Density, Temperature and Viscosity profiles used for the Reference Model at the initial state for an unperturbed column (blue lines) and for a column located at the center of the perturbation (green lines).

The coupling between the motion and the heat equation is given by the temperature dependence of density and viscosity for the lithospheric mantle and the asthenosphere. For simplicity, density and viscosity have constant values in the upper and lower crust (Table 2). We have considered a linear temperature-dependent density for the lithospheric mantle and the asthenosphere. The boundary between these two layers is assumed to be only thermal, with no compositional difference between them.

Table 2. Variable parameters used in each model. Density and viscosity of the upper and non-perturbed lower crust are shown in Table 1 since they are the same for all models.

model	**Orogenic Lower Crust**	**Lithospheric Mantle**			**Asthenosphere**		**Accumulated lateral migration after 30Ma of evolution**
	μ_{LC} (Pa s)	μ_{ref} (Pa s)	μ_{max} (Pa s)	μ_{mean} (Pa s)	μ_{ref} (Pa s)	μ_{mean} (Pa s)	(km)
RM	10^{20}	$2.5\text{x}10^{19}$	$2.5\text{x}10^{22}$	$1.46\text{x}10^{22}$	$2.5\text{x}10^{19}$	$5.07\text{x}10^{20}$	112
A	10^{19}	$2.5\text{x}10^{19}$	$2.5\text{x}10^{22}$	$1.46\text{x}10^{22}$	$2.5\text{x}10^{19}$	$5.07\text{x}10^{20}$	96
B	10^{21}	$2.5\text{x}10^{19}$	$2.5\text{x}10^{22}$	$1.46\text{x}10^{22}$	$2.5\text{x}10^{19}$	$5.07\text{x}10^{20}$	80
C	10^{20}	$2.5\text{x}10^{19}$	10^{22}	$6.36\text{x}10^{21}$	$2.5\text{x}10^{19}$	$5.07\text{x}10^{20}$	176
D	10^{20}	$2.5\text{x}10^{19}$	$5\text{x}10^{22}$	$2.71\text{x}10^{22}$	$2.5\text{x}10^{19}$	$5.07\text{x}10^{20}$	56
E	10^{20}	10^{19}	$2.5\text{x}10^{22}$	$1.33\text{x}10^{22}$	10^{19}	$2.03\text{x}10^{20}$	152
F	10^{20}	$5\text{x}10^{19}$	$2.5\text{x}10^{22}$	$1.57\text{x}10^{22}$	$5\text{x}10^{19}$	$1.01\text{x}10^{21}$	80

For the mantle, we have used a Newtonian temperature-dependent (exponential) viscosity law (Rüpke et al., 2004):

$$\mu(T,z) = \mu_0 \mu(z) \exp\left[b\left(\frac{T_0}{T} - 1 \right) \right] \tag{4}$$

$$\mu(z) = 1 + 124.5\left\{ 1 + \tanh\left[0.01\left(z - 450 \right) \right] \right\} \tag{5}$$

where μ_0 is a reference viscosity for each material; b is a parameter characterizing the temperature dependence of viscosity; and T_0 is the reference temperature at the base of the lithospheric mantle. The values of parameters common for all simulations are given in Table 1.

Assuming a Newtonian (linear) rheology has clear computational advantages and allows us to analyze the gross mechanical behavior, since it reproduces the continuum average properties of a discontinuous medium as a first approach. More-

over, the use of non-linear rheology in models with a high number of different materials would require consideration of an extraordinary high number of poorly constrained rheological parameters. Several authors have established that, due to the lithospheric mantle high strength at low (near surface) temperatures, only a thin layer with intermediate viscosity between the rigid mantle lithosphere and the asthenosphere can be quickly removed (e.g. Buck and Toksöz, 1983; Houseman and Molnar, 1997). To avoid this effect and promote the coherent behavior of the lithospheric mantle, an upper bound (μ_{max}) has been imposed to the mantle viscosity. This maximum value is reached at low temperatures, shallow depths, in the lithospheric mantle.

The values computed with such a temperature-dependent viscosity law should be envisaged as an effective viscosity whose variation we can control and modify easily in order to inspect its effect on the delamination mechanism. Assuming a non-linear rheology would make it more difficult to use the viscosity as a 'tuning' parameter, because the strong strain rate dependence would produce a more complex viscosity distribution.

1.2 Initial setup

Our initial setup (figure 1a) is inspired in a post collisional orogenic scenario, assuming the presence of an area of orogenic lithosphere, with both crustal and lithospheric roots. The modeled domain includes five layers: upper crust, non-perturbed lower crust, orogenic lower crust, lithospheric mantle and asthenosphere (i.e., the sub-lithospheric upper mantle). The orogenic root is designed following a sinus shape perturbation (e.g. Schott and Schmeling, 1998; Valera et al., 2008). The perturbed thickness of each layer doubles its non-perturbed thickness.

We have used the steady-state solution of the heat equation to compute the initial geotherm for the crust and lithospheric mantle, and an adiabatic initial temperature profile is assumed for the asthenosphere. In the orogenic zone, the isotherms are displaced downwards following the shape of the crustal and lithospheric roots (figure 1b).

We have assigned higher density values in the lower crust in the perturbed (orogenic) zone than in the non-perturbed zone. This increase in the 'orogenic' crust density can be related to the presence of eclogite and is consistent with previous numerical modeling of orogens (e.g., Schott and Schmeling, 1998; Jiménez-Munt et al., 2008). Figure 1b shows the viscosity and density profiles used for the Reference Model at the initial state. The viscosity values assumed in the rest of models are listed in Table 2.

We have imposed a narrow 'low viscosity conduit' of asthenospheric material connecting the lower crust with the asthenosphere adjacent to the orogenic root. Different authors have proposed several mechanism to justify the presence of this 'conduit', such as long lithospheric cracks, a hot rising 'plume' (Bird, 1979) or a volcanic line associated to previous subduction zone (Turcotte, 1983). All these mechanisms could explain the presence of a 'low viscosity conduit' filled with asthenospheric material. However, other authors have proposed that this 'conduit' is

filled with lithospheric material in which dehydration reactions coming from a previously subducted slab have lowered the viscosity on the lithosphere just above the slab (Schott and Schmeling, 1998; Arcay et al., 2007; Göğüş and Pysklywec, 2008). In order to check the influence of the nature of the 'low viscosity conduit', we also include a simulation in which the conduit is filled with weakened lithospheric material.

2. Results

2.1 Evolution of reference model

The characteristic evolution for the reference model of the delamination mechanism with lateral migration of the delamination point is shown in figure 2. Three stages can be clearly defined in the evolution of the delamination mechanism. The first stage initiates as the asthenospheric material rising through the conduit widens it, pushing the orogenic thickened crust and lithospheric root to the left. This stage lasts about 10 Ma.

The second stage lasts from 10 Ma to 18-20 Ma of evolution, corresponding to the full development of the delamination mechanism. The lateral intrusion of the asthenospheric material through the Moho accelerates, taking advantage of the low viscosity of the lower crust, peeling the lithospheric mantle off the crust. The leftward migration of the delamination pushes the thickened crust and produces crustal/lithospheric thickening in front of the migrating delamination point and crustal/lithospheric thinning behind it. The room vacated by the migrating lithospheric mantle is filled up by the ascent of asthenospheric mantle up to the Moho. At the same time, the denser lithospheric mantle sinks into the asthenosphere, dragging down lower crust material. This lithospheric foundering enhances the detachment of the lithospheric mantle from the crust, facilitating even more the lateral intrusion of the asthenospheric material.

The final stage is dominated by the sinking of the lithospheric material. Lower crust material is dragged down and forms a thin vertically elongated layer over the sinking lithospheric material, resembling the typical shape adopted by crust in an oceanic subduction zone.

As it has been described, the dynamics of the delamination mechanism is governed by the combination of the westward push exerted by the lateral intrusion of rising asthenospheric material and the downward force of the gravitational instability due to the mass excess of the lithospheric root, as in the convective removal mechanism. Therefore, the type of migrating process presented here lies in between two end-members: a process with strong lateral intrusion of asthenospheric material but without mass excess (kind of 'delamination sensu stricto' as was initially proposed by Bird 1978, 1979); and a process where a thickened lithospheric mantle develops a gravitational instability (i.e. convective removal, as proposed by Houseman at al., 1981).

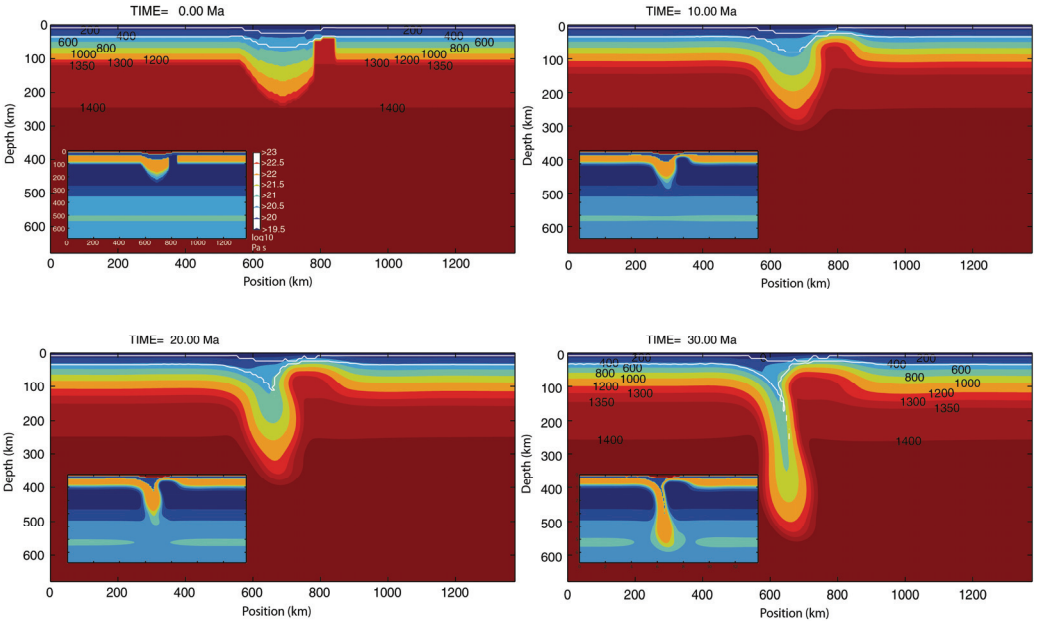

Figure 2: Evolution of the Reference Model for the delamination process with an 'asthenospheric conduit'. Colors represent temperature distribution with labels in ºC; white lines show the bases of the upper and lower crust. Insets show logarithm of viscosity (in Pa s) distribution.

2.2 Effect of viscosity

To describe the influence of viscosity structure on the delamination process and, in particular, on the lateral migration of the delamination point, we vary separately - within its typical range of plausible values- the viscosity of three different layers: lower crust, lithospheric mantle and asthenosphere.

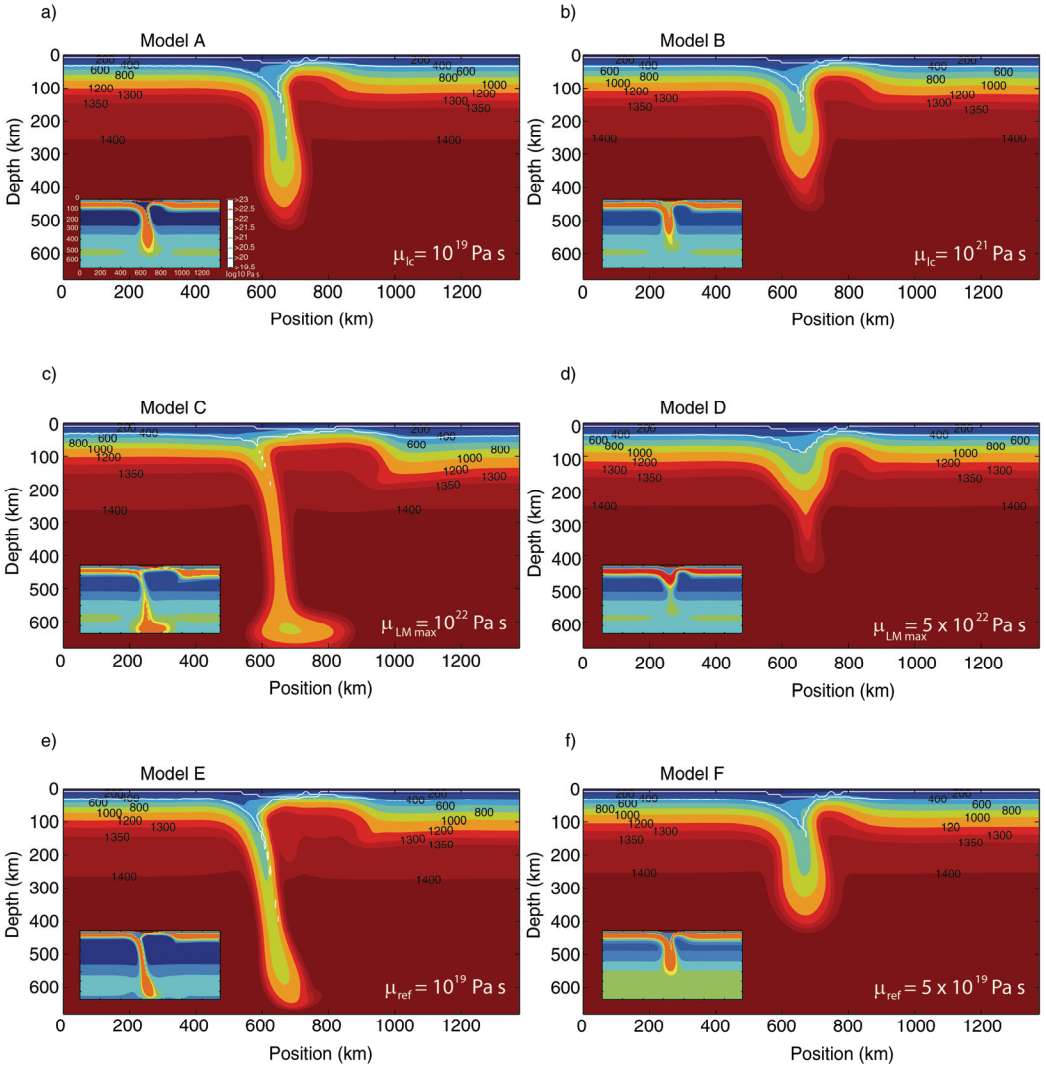

Figure 3: Final state after 30 Ma of evolution of several delamination models for different values of the viscosity. a) Model with decreased (with respect to RM) lower crust viscosity; b) Model with increased lower crust viscosity; c) Model with decreased upper bound for the viscosity of the lithospheric mantle (μ_{max}); d) Model with increased μ_{max}; e) Model with decreased reference viscosity for the asthenosphere and the lithosphere; f) Model with increased reference viscosity for the asthenosphere and the lithosphere. Colors represent temperature distribution with labels in ºC; white lines show the bases of the upper and lower crust. Insets show logarithm of viscosity (in Pa s) distribution. The scale for the viscosity is always the same as indicated in a).

Figure 3 shows the final state after 30 Ma of evolution of several models for different values of the viscosity. All other parameters are exactly the same as in the RM (see Table 2). Previous studies have proven that a low viscosity lower crust is needed to decouple the crust from the lithospheric mantle (e.g. Schott and Schmeling, 1998; Jull and Kelemen, 2001; Morency and Doin, 2004). It has been proposed that the low viscosity can be related to the presence of eclogite (e.g. Leech 2001; Jull and Kelemen, 2001; Lustrino, 2005). We vary the orogenic lower crust viscosity between 10^{19} Pa s and 10^{23} Pa s. As expected, high viscosities of the orogenic lower crust tend to hinder delamination, since a strong lower crust prevents the asthenosphere from expanding laterally along the Moho. Therefore, the conduit closes by thermal relaxation. This is in agreement with the statement by Morency and Doin (2004) that high Moho viscosities inhibit delamination propagation. Models with high viscosity orogenic lower crust (i.e. more than two orders of magnitude higher than RM) present no delamination at all. In these models the perturbation drips 'in situ', with insignificant lateral migration of the delamination point, similar to the convective removal mechanism. Therefore, we also find that the presence of a low viscosity layer in the crust is crucial to enable the lateral propagation of delamination.

It might be surprising to obtain that lower viscosities of the orogenic lower crust (model A, figure 3a, with a viscosity ten times lower than in RM) cause less migration of the delamination point than the RM, although the difference is small (Table 2). Based on these models, we interpret that, for this case, the lower crust is so soft that the crust and the lithospheric mantle are decoupled. This decoupling produces that sinking becomes more effective than the lateral push of intruding asthenosphere, so lithospheric perturbation tends to drip 'in situ' (figure 3a).

We have performed several models with different values for the imposed maximum mantle viscosity, μ_{max}. High values of this maximum inhibit propagation of delamination. Model with a maximum value of $5x10^{22}$ Pa s (model D in figure 3d), higher than the maximum value of $2.5x10^{22}$ Pa s used in the RM, presents very little lateral migration of the delamination point (Table 2) and the conduit tends to close, while the perturbation sinks 'in situ'. In contrast, a more mobile lithospheric mantle, with lower values of this maximum viscosity, is more easily separated from the crust by the horizontal intrusion of asthenosphere (model C in figure 3c). Therefore, it yields higher displacements of the delamination point and earlier development of delamination. The mean viscosity value of the lithospheric mantle is $6.4x10^{21}$ Pa s for model C (figure 3c) and $2.7x10^{22}$ Pa s for model D (figure 3d). The strong difference in the results obtained with such small variations shows that the process is very sensitive to this maximum bound.

In order to explore the effect of the asthenospheric viscosity, we vary the reference value (μ_0) for the mantle viscosity. The mean viscosity values of the asthenosphere obtained vary from $2.0x10^{20}$ Pa s for model E (figure 3e) to $1.0x10^{21}$ Pa s for model F (figure 3f). Figure 3e shows that asthenospheric viscosities lower (model E) than in the RM produce higher displacements of the delamination point and earlier development of delamination. In contrast, higher viscosities of the asthenosphere

result in a slower delamination process (figure 3f), with little displacement of the delamination point. We therefore obtain that the lower the asthenosphere viscosity, the faster the process evolves, since a very mobile asthenospheric material is able to laterally intrude and displace the lower crust material more easily than a stiffer asthenosphere.

Although all these results have been obtained considering a linear rheology, we expect that the effects observed do not qualitatively change with non-linear rheology. According to previous studies, non-linear rheology tends to localize deformation since viscosity is reduced as strain rates increases (e.g. Christensen, 1984; Houseman and Molnar, 1997; Gemmer and Houseman, 2007; Göğüş and Pysklywec, 2008). This viscosity reduction is predicted to occur mainly in the lower crust, where the strain rates should be higher. Therefore, this viscosity reduction is expected to favor the delamination mechanism.

2.3. Effect of radiogenic heat production

Figure 4 shows the crustal structure and temperature distribution after 30 Ma of evolution for models which differ only in the crustal radiogenic heat production (RHP). Mantle heat production is neglected because of the low concentration of radioactive elements in peridotides. These variations of heat production cause variations in the initial geotherm, but the initial lithospheric thickness and temperature at the base of the lithosphere (1350ºC) are imposed to be the same for all models. Values of initial Moho temperature and surface heat flow (SHF) for each model are indicated in Table 3.

Table 3. Variable parameters used in each model. Other parameters else are identical to the Reference Model.

Model (fig)	$\mathbf{H_{UC}}$ (W/m^3)	$\mathbf{H_{LC}}$ (W/m^3)	$\mathbf{T_{Moho}}^*$ **(ºC)**	**SHF** * (mW/m^2)	**Maximum depth of 1350ºC isotherm** (km)
G1 (fig 4.a)	1.0	0.1	488.5	43.31	600
RM (fig4.b)	1.5	0.1	533.7	54.51	544
G2 (fig4.c)	2.0	0.1	578.8	65.70	488
G3 (fig 4.d)	1.5	0.05	494.1	51.62	592
G4 (fig4.3)	1.5	0.3	621.7	60.93	464
G5 (fig4.f)	1.5	0.8	841.7	77.00	352

* computed at t=0 Ma, at the axis of the perturbation

While the effect of varying crustal RHP on the amount of asthenospheric upwelling and on lateral migration of the delamination point is small, the effect on the resulting geometry of the detached lithospheric mantle is dramatic, as evidenced by the different maximum depth reached by the 1350ºC isotherm for each model (Table 3). The effect of upper crust RHP is explored in models shown in figure 4a-c

(model in figure 4b corresponds to the Reference Model). The lithospheric mantle in the model with a relatively high upper crust RHP (Model G2 figure 4c) is warmer and less negatively buoyant than models with lower upper crust RHP (Model G1 in figure 4a) and therefore reaches shallower depths.

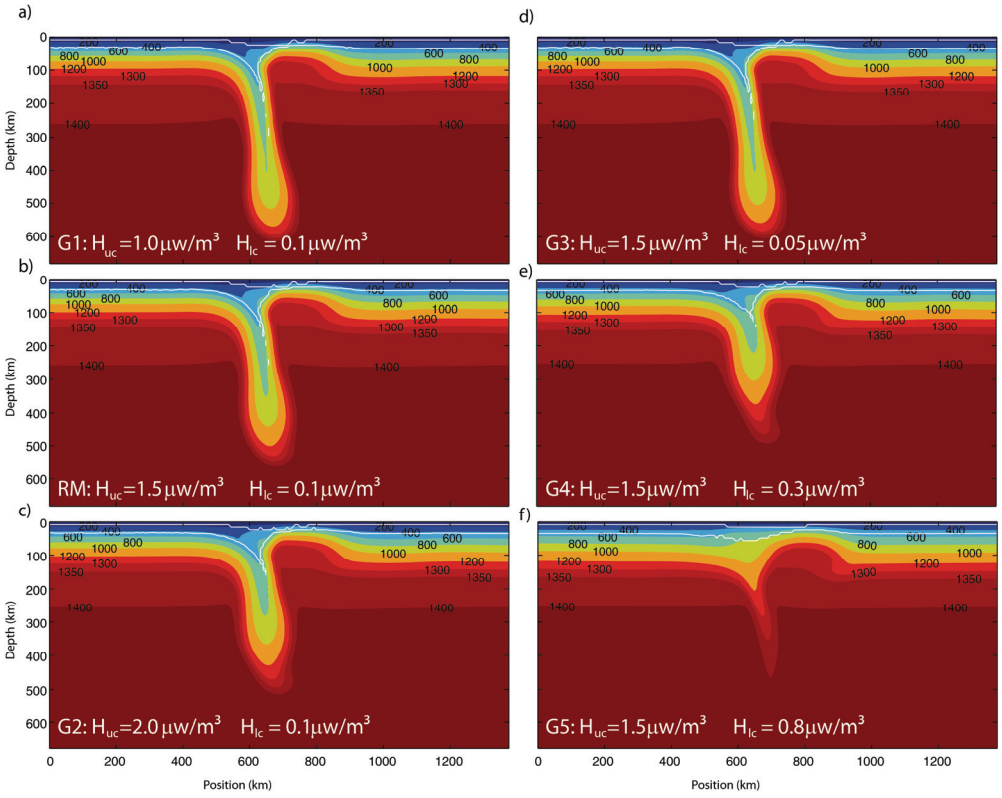

Figure 4: Final state after 30 Ma of evolution of several delamination models for different values of the radiogenic heat production (H). All other parameters else are the same as in Reference Model. a-c) shows the influence of increasing the upper crust radiogenic heat production with constant H for the lower crust. d-f) shows the influence of increasing lower crust radiogenic heat production with constant H for the upper crust. Model b) coincides with the Reference Model. Colors represent temperature distribution with labels in ºC; white lines show the bases of the upper and lower crust.

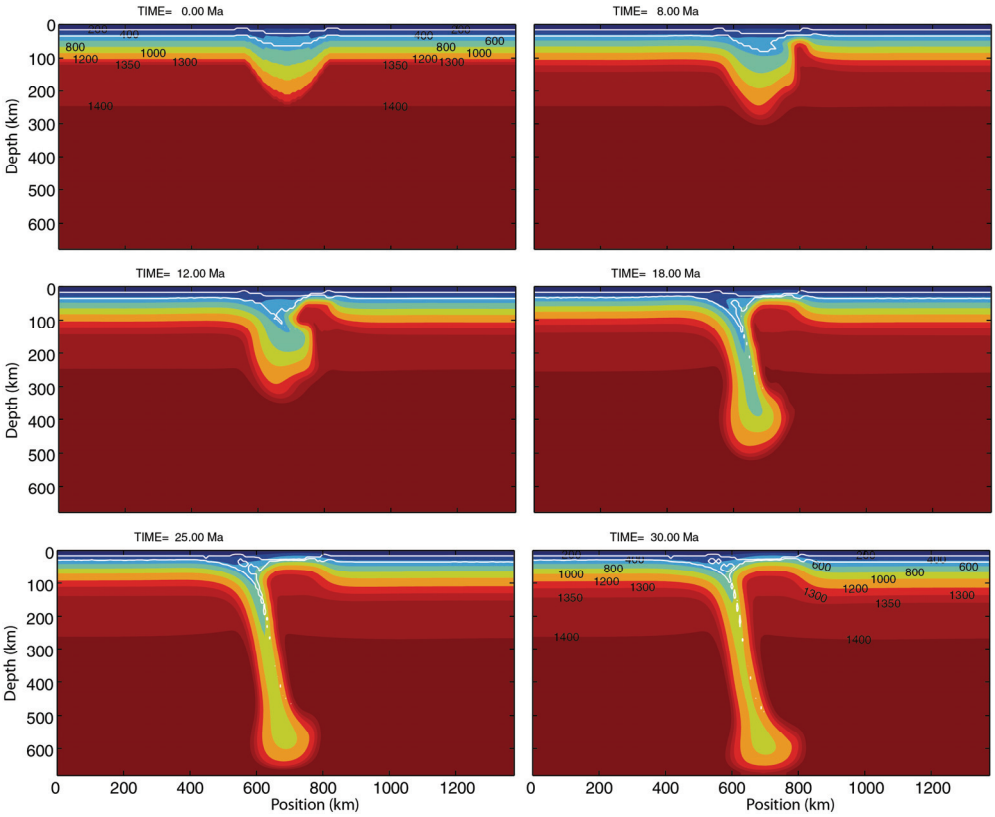

Figure 5: Evolution of a delamination process with a 'low viscosity lithospheric conduit'. Colors represent temperature distribution with labels in ºC; white lines show the bases of the upper and lower crust. Initial setup is exactly the same as in Reference Model, only varying the nature of the material filling the 'conduit'.

Models G3-G5 (figure 4d-f) have the same upper crust RHP as the RM, whereas the lower crust RHP varies between end-member values representative for lower crust granulite facies. Vilà et al., (2010) present a new compilation of RHP values distributed according to the main lithosphere rock types, and recommend an average RHP of 0.15 μWm^{-3} for mafic granulites, 0.35 μWm^{-3} for intermediate granulites and 0.85 μWm^{-3} for felsic granulites. Following Vilà et al., (2010), eclogites show lower variability than granulites, with a mean value around 0.25 μWm^{-3} (similar to model G4 in figure 4e). The RHP value of 1.5 μWm^{-3} adopted for upper crust is assumed to be representative for low-medium grade metamorphics (whereas 1 μWm^{-3} is representative for tonalites and 2 μWm^{-3} for granodiorites). The thermal negative buoyancy of the lithospheric mantle is significantly reduced when increasing lower crust RHP (compare models G3-G4-G5). Interestingly the sinking lithospheric mantle is thermally assimilated in the surrounding asthenosphere and a

slab-like structure is not created (model G5 in figure 4f). This result can provide an explanation for areas where removal of lithospheric material is inferred, but a slab-like large scale structure is not found in the upper mantle (e.g. Tibet plateau and eastern Anatolia).

2.4. Effect of the nature of the 'conduit'

Regarding the nature of the conduit, figure 5 shows the evolution of a model in which the conduit is formed of low viscosity lithospheric material. The maximum viscosity of the conduit in this model is fixed to be 10^{20} Pa s. This condition yields a 'low viscosity lithospheric conduit', with viscosity values ranging from identical to the surrounding values at the bottom of the conduit, to two orders of magnitude less than the surroundings at the top of the conduit. However, it is still initially more viscous than the 'asthenospheric conduit'.

Thermal structure does not show any conduit at the initial state as the temperature of the 'low viscosity lithospheric conduit' is the same as the surrounding lithospheric mantle (figure 5a). The process is qualitatively the same as in the RM. At the beginning, the 'low viscosity lithospheric conduit' is heated by asthenospheric upwelling and after 8 Ma (figure 5b) the thermal distribution resembles the initial thermal distribution of the RM. Then a fast lateral migration of the delamination point occurs (figure 5c) and the root grows and sinks (figure 5d), reaching the base of the upper mantle after 25 Ma (figure 5e). In the RM, this development is slower since the asthenosphere in contact with lower crust cools, and, therefore, its viscosity increases, creating a high viscosity thin 'barrier' (see insets representing viscosity in figure 2).

3. Concluding remarks

Lateral migration of the delamination point is shown here to be very sensitive to the lithospheric mantle viscosity and, to a lesser degree, to asthenosphere viscosity. An increase of only one order of magnitude in the maximum viscosity of the lithospheric mantle (from 10^{22} to 10^{23} Pa s) causes a change from a well-developed delamination with large displacement of delamination point to a complete inhibition of this process. Development of the delamination mechanism is also favored by low viscosity lower crust, which is likely related to the presence of eclogite in an orogenic lower crust.

Varying crustal RHP is shown to have little influence on the amount of asthenospheric upwelling and on lateral migration of delamination. In contrast, the effect on the resulting geometry of the detached lithospheric mantle is dramatic. Models with very high lower crust RHP reproduce asthenospheric upwelling, but the sinking lithospheric mantle is thermally assimilated in the surrounding asthenosphere without creating a slab-like structure in the upper mantle.

We have tested the effect of the nature of the material forming the low viscosity zone adjacent to the lithospheric root. We obtain that the nature of the conduit, either formed of low viscosity lithospheric mantle or asthenospheric material, does not significantly affect the development of delamination. We therefore suggest that

both lithospheric weakening by dehydration processes and thermal thinning processes during previous subduction episodes are plausible mechanisms for the formation of 'low viscosity conduits' triggering delamination.

4. Acknowledgments

This work was funded by the Spanish Plan Nacional del MCINN project CGL2009-13103; and funding from UCM Research Groups. This is a contribution of the Consolider-Ingenio 2010 team CSD2006-00041 (TOPO-IBERIA). Calculations were partially carried out in the Fiswulf cluster of the Faculty of Physics.

References

ANDERSON, J. D., (1995), Computational fluid dynamics, McGraw Hill, Inc.

ARCAY, E., E. TRIC, AND M.-P. DOIN (2007), Slab surface temperature in subduction zones: Influence of the interplate decoupling depth and upper plate thinning processes. *Earth Planet. Sci. Lett.,* 255, 324–338, http://dx.doi.org/10.1016/j.epsl.2006.12.027

BIRD, P. (1978), Initiation of intracontinental subduction in the Himalaya. *J. Geophys. Res.,* 83, 4975-4987, http://dx.doi.org/10.1029/JB083iB10p04975

BIRD, P. (1979), Continental delamination and the Colorado Plateau. *J. Geophys. Res.,* 84, 7561-7571.

BUCK, W.R. AND M.N. TOKSÖZ, (1983), Thermal effects of continental collisions: Thickening a variable viscosity lithosphere, *Tectonophysics,* 100, 53-69, http://dx.doi.org/10.1016/0040-1951(83)90178-6

CHRISTENSEN, U. R., (1984), Convection with pressure- and temperature- dependent non-Newtonian rheology, *Phys. J. R. Astro. Soc.,* 77, 343-384, http://dx.doi.org/10.1111/j.1365-246X.1984.tb01939.x

ENGLAND, P.C. AND G. A. HOUSEMAN (1989), Extension during continental convergence, with application to the Tibetan Plateau, *J. Geophys. Res.,* 94, 17561-17579, http://dx.doi.org/10.1029/JB094iB12p17561

GEMMER, L. AND G. A. HOUSEMAN (2007), Convergence and extension driven by lithospheric gravitacional instability: evolution of the Alpine–Carpathian–Pannonian SYSTEM. *GEOPHYS. J. INT., 168,* 1276-1290.

GÖĞÜŞ, O. H. AND R. N. PYSKLYWEC (2008), Near-surface diagnostics of dripping or delaminating lithosphere, *J. Geophys. Res.,*113, B11404, http://dx.doi.org/10.1029/2007JB005123

HOUSEMAN, G., D. MACKENZIE AND P. MOLNAR, (1981), Convective instability of a thickened boundary layer and its relevance for the thermal evolution of continental belts, *J. Geophys. Res*., 86, B7, 6115-6132, http://dx.doi.org/10.1029/JB086iB07p06115

HOUSEMAN, G. AND P. MOLNAR (1997), Gravitational (Rayleigh–Taylor) instability of a layer with non-linear viscosity and convective thinning of continental lithosphere, *Geophys. J. Int.,* 128, 125–150, http://dx.doi.org/10.1111/j.1365-246X.1997.tb04075.x

JIMÉNEZ-MUNT I., M. FERNÀNDEZ, J. VERGÉS AND J.P. PLATT, (2008), Lithosphere structure underneath the Tibetan Plateau inferred from elevation, gravity and geoid anomalies, *Earth. Planet. Sci. Lett.,* 267, 276-289, http://dx.doi.org/10.1016/j.epsl.2007.11.045

JULL, M., AND P. B. KELEMEN (2001), On the conditions for lower crustal convective instability, *J. Geophys. Res.,* 106(B4), 6423–6446, http://dx.doi.org/10.1029/2000JB900357

LEECH, M.L. (2001), Arrested orogenic development: eclogitization, delamination, and tectonic collapse. *Earth Planet. Sci. Lett.,* 185, 149-159, http://dx.doi.org/10.1016/S0012-821X(00)00374-5

LUSTRINO, M. (2005), How the delamination and detachment of lower crust can influence basaltic magmatism, *Earth-Sci. Rev.,* 72, 21–38, http://dx.doi.org/10.1016/j.earscirev.2005.03.004

MORENCY, C., Y DOIN, M.-P. (2004), Numerical simulations of the mantle lithosphere delamination, *J. Geophys. Res.,* 109, B03410, http://dx.doi.org/10.1029/2003JB002414

RÜPKE, L.H., PHIPPS- MORGAN, J., HORT, M., AND CONNOLLY, J. A. D. (2004), Serpentine and the subduction zone water cycle, *Earth Planet. Sci. Lett.,* 223, 17-34, http://dx.doi.org/10.1016/j.epsl.2004.04.018

SCHOTT, B., AND SCHMELING, H. (1998), Delamination and detachment of a lithospheric root, *Tectonophysics,* 296, 225-247, http://dx.doi.org/10.1016/S0040-1951(98)00154-1

TURCOTTE, L. (1983): Mechanisms of crustal deformation. *Journal of the Geological Society of London,* 140: 701-724, http://dx.doi.org/10.1144/gsjgs.140.5.0701

VALERA, J. L., A. M. NEGREDO AND A. VILLASEÑOR, (2008), Asymmetric delamination and convective removal numerical modeling: Comparison with evolutionary models for the Alboran Sea region, *Pure appl. geophys.,* 165, 1683–1706, http://dx.doi.org/10.1007/s00024-008-0395-8

VALERA, J. L. (2009), Development and application of numerical thermomecanical modeling of continental delamination processes. PhD thesis (in Spanish), Univ. Complutense de Madrid, 224pp, http://eprints.ucm.es/9824/

VALERA, J. L., NEGREDO, A. M. Y JIMÉNEZ-MUNT, I, (2011), Deep and near-surface consequences of root removal by asymmetric continental delamination, *Tectonophysics,* 502, 257-265, http://dx.doi.org/10.1016/j.tecto.2010.04.002

VILÀ, M., M. FERNÁNDEZ, I. JIMÉNEZ-MUNT, (2010) Radiogenic heat production variability of some common lithological groups and its significance to lithospheric thermal modeling, *Tectonophysics*, 490, 152–164, http://dx.doi.org/10.1016/j.tecto.2010.05.003